Mechanical and Thermal Properties of Polyimide/Silica Hybrids with Imide-Modified Silica Network Structures

Muhammad Khalil,[1] Shaukat Saeed,[1] Zahoor Ahmad[2]

[1]*Department of Chemical and Materials Engineering, Pakistan Institute of Engineering and Applied Sciences, Islamabad 45650, Pakistan*
[2]*Department of Chemistry, Faculty of Science, Kuwait University, P.O. Box 5969, Safat 13060, State of Kuwait*

Received 17 January 2007; accepted 31 July 2007
DOI 10.1002/app.27149
Published online 9 October 2007 in Wiley InterScience (www.interscience.wiley.com).

ABSTRACT: A series of hybrid materials incorporating imide-modified silica (IM-silica) network structures into a polyimide (PI) matrix were produced with a sol–gel technique from solution mixtures of poly(amic acid) and tetraethoxysilane (TEOS) containing alkoxysilane-terminated amic acids with various degrees of polymerization. The hybrid films, obtained by solvent evaporation, were heated successively to a maximum temperature of 300°C to carry out the imidization process and silica network formation in the PI matrix. The morphology and mechanical properties of these hybrids with IM-silica networks were studied and compared with the properties of one in which reinforcement of the matrix was achieved with a pure silica network generated from TEOS. The introduction of longer imide spacer groups into the silica network led to a drastic decrease in the silica particle size. Improved tensile modulus was observed in such compatibilized hybrid systems. Comparative thermogravimetric measurements of these hybrids showed improved thermooxidative resistance. A PI hybrid with 30% IM-silica had a thermal decomposition temperature nearly 260°C higher than that of the pure PI matrix. The high surface area of the interconnected silica domains and increased interfacial interaction were believed to restrict the segmental motion of the polymer and thus slow the diffusion of oxygen in the matrix, thereby slowing the oxidative decomposition of the polymer. The reinforcement of existing and new PIs by this method offers an opportunity for improving their thermooxidative stability without degrading their mechanical strength. © 2007 Wiley Periodicals, Inc. J Appl Polym Sci 107: 1257–1268, 2008

Key words: compatibilization; mechanical properties; nanocomposites; polyimides; thermal properties

INTRODUCTION

The search for organic polymers resistant to high temperatures has been the subject of numerous studies focused primarily on extending the service life of components exposed to harsh environments.[1] The most prominent among thermally stable organic polymers are aromatic polyimides (PIs). In addition to excellent thermal and thermooxidative stability, their other outstanding characteristics, such as superior chemical resistance, a low dielectric constant, and high tensile strength and modulus, make them excellent candidates for use as insulating materials for electronics, high-performance gas-separation membranes, high-temperature adhesives and coatings, and matrices for composites.[1–4] Even though PIs are thermally very stable polymers, they can still degrade if exposed to a high temperature for a long period. This exposure can lead to changes in the physical and/or chemical structure of the materials and affect their thermooxidative stability.[5] A technology that has been gaining attention in recent years is the incorporation of nanoscale inorganic components into organic polymers as a means of improving their mechanical properties and stability.[6–9] These nanohybrids possess unique properties typically not shared by conventional composite materials.

PI/silica materials offering favorable properties of both components are, therefore, in great demand for high-performance/high-temperature applications. The sol–gel process is a reasonably good approach for producing fine silica particles uniformly dispersed in the PI matrix through *in situ* polymerization of monomeric precursors. Thermodynamic immiscibility between inorganic and organic materials, however, may lead to phase separation of the components. Often, as a result, micrometer-sized silica particles appear in the resultant hybrids. To make optically clear hybrid films, the size of filler particles should be far below the micrometer scale. The small size of filler phase domains in hybrids also leads to an exceptionally large domain interface that controls the degree of interaction between the filler and polymer and, therefore, the properties.[10] To implement the novel properties of hybrids;

Correspondence to: M. Khalil (mkminhas@pieas.edu.pk).
Contract grant sponsor: Higher Education Commission of Pakistan (under the Indigenous Ph.D. Research Scheme).

Journal of Applied Polymer Science, Vol. 107, 1257–1268 (2008)
© 2007 Wiley Periodicals, Inc.

processing methods that lead to controlled particle size, distribution, dispersion, and interfacial interactions are therefore critical. Various methods used to control the phase separation have been discussed by Ahmad and Mark,[11,12] Wen and Wilkes,[13] and Mascia,[14] among others. A number of researchers[7,15–29] in separate studies have prepared bonded PI/silica hybrids using tetraalkoxysilane with different aminoalkoxysilanes. They have found that both the amino and alkoxy groups on these silanes enable chemical bonding between organic and inorganic networks, resulting in the formation of more homogeneous and transparent films in comparison with those prepared with tetraalkoxysilane only. Hybrid films in general show better mechanical and thermal properties.

A recent study,[30,31] however, has reported the preparation of PI/silica hybrids by the modification of the silica network itself with aromatic diimide linkages. The morphology of the resulting PI/silica hybrids showed a much finer distribution of nanometer-size silica particles with diffused boundaries. The inclusion of a thermally stable imide linkage in the silica network produced hybrids with better optical, mechanical, and thermal properties.

In this work, we prepared a series of hybrid materials by incorporating organically modified silica network structures into a poly(amic acid) (PAA) solution, a PI precursor. The silica network structure used for reinforcement was modified with imide linkages varying in chain length. The hybrid films after the imidization and the sol–gel process were characterized for their morphology, mechanical properties, and thermooxidative resistance, and the effect of introducing imide spacer groups of different sizes into the silica network on these properties is explained.

EXPERIMENTAL

Chemicals

Pyromellitic dianhydride (PMDA; 99.2%; Sigma-Aldrich Inc., St. Louis, MO), 4,4′-oxydianiline (ODA; 99.9%; Sigma-Aldrich Inc., St. Louis, MO), *p*-aminophenyltrimethoxy silane (APTMOS; 95%; ABCR GmbH & Co., Karlsruhe, Germany), tetraethoxysilane (TEOS; 97.5%; Acros Organics, Fair Lawn, NJ), and dimethylacetamide (DMAc; 99.8%, water content $< 0.005\%$; Aldrich) were used as received.

Preparation of PAA

PAA was prepared by the reaction of high-purity monomers with anhydrous DMAc as a solvent. In a 1-L, three-necked flask fitted with a mechanical stirrer, 25.1325 g (0.1254 mol) of ODA and 240 g of DMAc were placed, and the contents were stirred until a clear solution of diamine was obtained. Then,

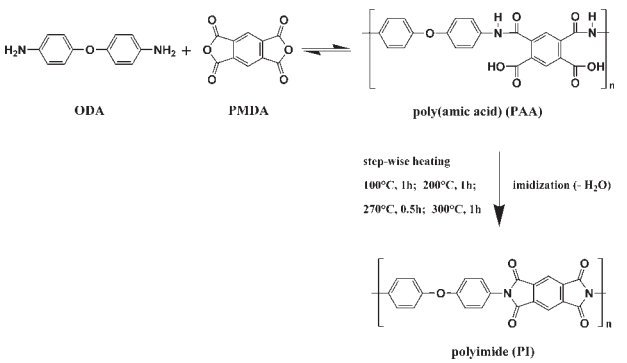

Figure 1 Synthesis of PAA and its conversion to PI.

27.5753 g (0.1254 mol) of PMDA was added to the amine solution with continued stirring. As the polymerization reaction proceeded, 594 g of DMAc was further added to the reaction mixture to facilitate the stirring and to obtain a 6 wt % PAA solution. The solvent and the monomer PMDA were extremely sensitive to moisture, and therefore the polymerization reactions were carried out under completely anhydrous conditions around 5°C. Such conditions were achieved with a sealed glovebox having forced circulation of air in a closed loop over dried calcium chloride and directed on a refrigeration plate fitted within the glovebox. The refrigeration plate, maintained at −15°C, served to condense any moisture remaining in the air and to lower the temperature of the reaction environment. After 12 h of continued stirring, 1% PMDA in excess to that stoichiometric value was added just to compensate any loss of functionalities due to its hygroscopic nature. The reaction was assumed to be complete after 30 h of polymerization. The reaction scheme for the preparation of PAA is shown in Figure 1.

Preparation of the imide-modified silica (IM-silica) network

For the preparation of the imide-modified silica (IM-silica) network, alkoxysilane-terminated amic acids (AAs) having various degrees of polymerization were prepared by the adjustment of the stoichiometry of PMDA, ODA, and APTMOS. Three types of AAs end-capped with silane were prepared with PMDA and a mixture of diamines and monoamines, that is, ODA and APTMOS solutions in DMAc. The amine solution was added dropwise to the PMDA solution with constant stirring to keep final PMDA/ODA/APTMOS molar ratios of 1 : 0 : 2, 2 : 1 : 2, and 3 : 2 : 2 in the reaction mixture to produce alkoxysilane-terminated diamic acids, tetraamic acids, and hexaamic acids, respectively. The reaction mixtures were stirred further for 4 h, and then a measured amount of a TEOS solution in DMAc (40 wt %) was added to these mixtures with continuous stirring.

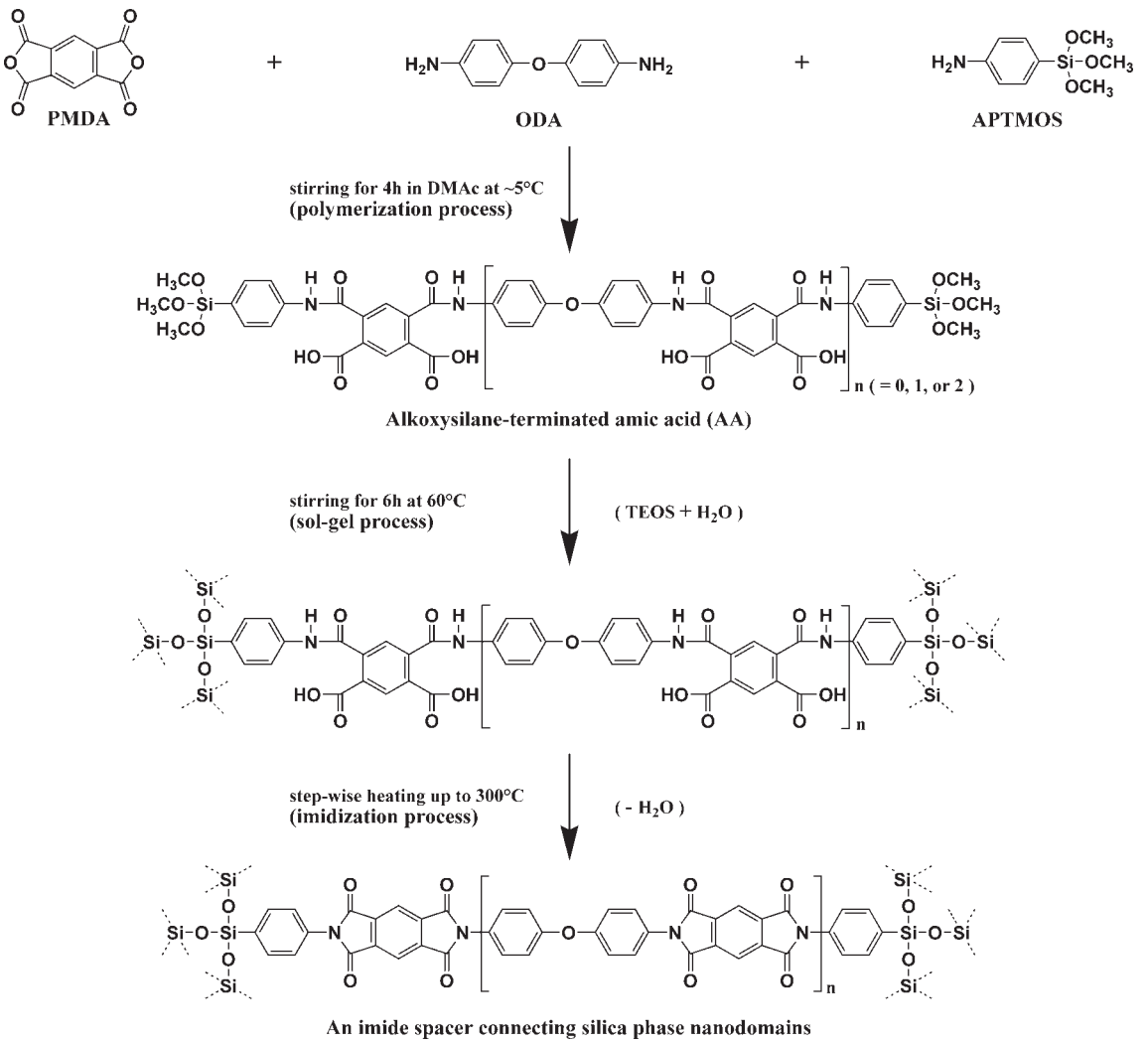

Figure 2 IM-silica network formation with APTMOS.

The amount of TEOS was adjusted, in each case, to derive 95% silica from TEOS and 5% from APTMOS present at the end groups of AAs during the sol–gel process. The reaction scheme for the preparation of the IM-silica network is illustrated in Figure 2.

Preparation of the PI/unmodified silica (UM-silica) hybrid films

A TEOS solution (10 wt %) in DMAc was added in a required amount to a PAA solution, and the sol–gel process was carried out at 60°C to generate pure silica networks ranging from 5 to 40 wt % in the matrix. The general scheme for the hydrolysis/condensation reactions (sol–gel process) of TEOS leading to the formation of pure or UM-silica networks is shown in Figure 3. The hybrid films were prepared by the solvent elution technique. These films were heated successively at 100, 200, 270, and 300°C for 1 h, 1 h, 30 min, and 1 h, respectively, to carry out the imidization process (Fig. 1). A flow-sheet diagram for the preparation of PI/UM-silica hybrid films (U series) is shown in Figure 4, and their compositions are given in Table I.

Preparation of the PI/IM-silica hybrid films

A mixture of TEOS and alkoxysilane-terminated AA solutions in DMAc was added in a required amount to a PAA solution, and the sol–gel process was carried out at 60°C to generate a polymer-modified silica network in the matrix. The hybrid films were prepared by the solvent elution technique and imidized by heating up to 300°C as described earlier. These PI hybrid systems are designated 1B, 2B, and 3B, which correspond to diimide, tetraimide, and hexaimide chains, respectively, used to modify the silica network structure in the matrix. The flow-sheet diagram for the preparation of PI/IM-silica hybrid films (1B, 2B, and 3B series) is shown in Figure 5, with the composition of the hybrids given in Table I.

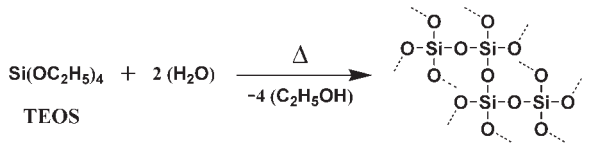

Figure 3 Sol–gel process leading to the formation of the pure silica network.

Characterization of the hybrid films

Fourier transform infrared (FTIR) analysis of the pure PI, PI/UM-silica, and PI/IM-silica hybrid films was carried out in the range of 550–4000 cm^{-1} with a Nicolet (ThermoFisher Scientific Inc., Waltham, MA) 6700 attenuated total reflection (ATR)–FTIR spectrophotometer. The morphology of the hybrid films was studied with a Leo (Leo Electron Microscopy Group, Oberkochen, Germany) 1550 Schottky field emission scanning electron microscopy (FESEM) microscope. The samples were fractured in liquid nitrogen, sputter-coated with gold, and mounted on aluminum mounts. Secondary electron images were taken with an in-lens detector. The tensile measurements were taken on a Testometric (Rochdale, Lancashire, UK) Micro-500 machine at a uniform strain rate of 5 mm/min with a 1-kN load cell. All the samples were dried at 120°C overnight before the testing. From the stress–strain data measured at 25°C, the ultimate tensile strength and tensile modulus were calculated. The reported values are the averages of five specimens in each case. The thermal oxidative stability of the samples, based on their decomposition profiles in air, was measured by thermogravimetry with a PerkinElmer (Shelton, CT) Diamond thermogravimetric/differential thermal analyzer (TG/DTA). Thermogravimetric runs were conducted on samples (~8 mg) punched from the film as equal-diameter circular pieces with an average weight of ~2 mg. All the specimens were dried for 24 h at 120°C before analysis. The instrument was programmed to heat the specimen from the ambient temperature to 200°C at a rate of 10°C/min, maintain the temperature at 200°C for 30 min, and then heat it to 1000°C at a constant heating rate of 10°C/min. During the analysis, the sample chamber of the instrument was kept under atmospheric air, whereas the region of the microbalance mechanism was maintained under dry nitrogen and purged at a rate of 0.02 L/min. Thermal curves were used to compare the decomposition behavior of the synthesized hybrids in thermooxidative environments.

RESULTS AND DISCUSSION

The conversion of PAA/AA to PI/imide and the formation of the silica phase in the hybrid systems were determined with ATR–FTIR spectroscopy. The normalized FTIR spectra at 1497 cm^{-1} (aromatic ring stretching) of pure PI and the PI/silica hybrids (U, 1B, 2B, and 3B series) are shown in Figure 6. The characteristic absorption peaks of the imide ring can be observed at 1773–1776 (C=O asymmetrical stretching), 1715–1717 (C=O symmetrical stretching), 1368–1375 (C—N stretching), and 720–722 cm^{-1} (C=O bending). A broad band can be observed at 1020–1104 cm^{-1} in the spectra of the U, 1B, 2B, and 3B series, and it gradually increases in intensity with increasing silica content. This band can be attributed to the asymmetric stretching mode of the Si—O—Si group and is indicative of the formation of the Si—O—Si network in the hybrid films. It can be noted from Figure 6 that the absorption peaks of 1B20, 2B20, and 3B20 are skewed toward the higher frequency side and those of 1B30, 2B30, and 3B30 are shifted to the lower frequency side of the ν_{as} (Si—O—Si) region. However, the spectrum of U30 shows a broad distribution in this frequency range. The study conducted by Musto et al.[32] demonstrated that ν_{as} (Si—O—Si) absorption appears at lower wave numbers for linear SiO_2 structures and at

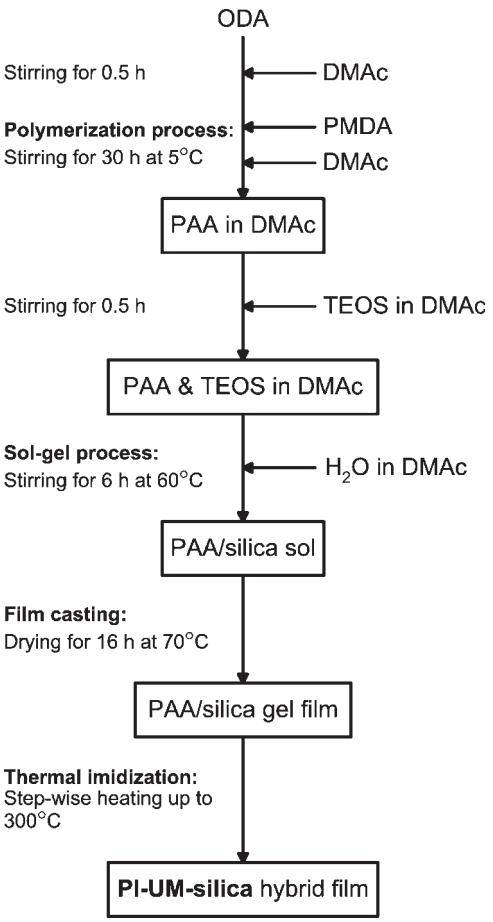

Figure 4 Scheme for the preparation of the PI/UM-silica hybrid (U series) films.

TABLE I
Synthesized Series of PI/Silica Hybrid Films with an Average Thickness of 138 ± 20 μm

Series[a]	Code	APTMOS : TEOS (molar ratio)	Film composition (wt %)			Status[b]	Residue at 1000°C (wt %)[c]
			Silica	Imide spacer	PI		
Matrix	PI	0 : 0	0	0	100	F, T	0.00
U	U05	0 : 1	5.00	0	95.00	F, T	3.84
	U10	0 : 1	10.08	0	89.92	F, T	9.54
	U15	0 : 1	15.03	0	84.97	F, O	13.27
	U20	0 : 1	20.01	0	79.99	F, O	18.73
	U25	0 : 1	25.01	0	74.99	F, O	24.32
	U30	0 : 1	30.92	0	70.08	F, O	30.77
	U40	0 : 1	40.00	0	60.00	B, O	—
1B	1B05	0.05 : 0.95	5.04	0.78	94.18	F, T	3.36
	1B10	0.05 : 0.95	10.02	1.54	88.44	F, T	9.12
	1B15	0.05 : 0.95	14.97	2.30	82.73	F, T	14.51
	1B20	0.05 : 0.95	20.00	3.08	76.92	F, T	19.05
	1B25	0.05 : 0.95	24.97	3.85	71.18	F, T	24.40
	1B30	0.05 : 0.95	30.06	4.63	65.31	F, T	29.14
	1B40	0.05 : 0.95	39.87	6.15	53.98	F, T	—
2B	2B05	0.05 : 0.95	5.08	1.59	93.33	F, T	3.55
	2B10	0.05 : 0.95	10.06	3.14	86.80	F, T	8.52
	2B15	0.05 : 0.95	15.00	4.69	80.31	F, T	13.72
	2B20	0.05 : 0.95	20.05	6.26	73.69	F, T	18.76
	2B25	0.05 : 0.95	25.00	7.80	67.20	F, T	23.64
	2B30	0.05 : 0.95	29.99	9.37	60.64	F, T	29.09
	2B40	0.05 : 0.95	39.71	12.40	47.89	F, T	—
3B	3B05	0.05 : 0.95	5.32	2.50	92.18	F, T	3.67
	3B10	0.05 : 0.95	10.06	4.71	85.23	F, T	9.89
	3B15	0.05 : 0.95	15.05	7.06	77.89	F, T	13.56
	3B20	0.05 : 0.95	20.01	9.38	70.61	F, T	19.12
	3B25	0.05 : 0.95	25.02	11.72	63.26	F, T	22.90
	3B30	0.05 : 0.95	30.02	14.07	55.91	F, T	28.24
	3B40	0.05 : 0.95	39.76	18.63	41.61	B, T	—

[a] The U series represents the PI/silica hybrids with a pure silica network (generated with TEOS) as a reinforcement. The 1B series represents the PI/silica hybrids with a diimide-modified silica network as a reinforcement. The 2B series represents the PI/silica hybrids with a tetraimide-modified silica network as a reinforcement. The 3B series represents the PI/silica hybrids with a hexaimide-modified silica network as a reinforcement.
[b] F = flexible; T = transparent; O = opaque; B = brittle.
[c] Measured by thermogravimetry at a heating rate of 10°C/min in atmospheric air.

higher wave numbers for cyclic SiO_2 structures. Therefore, in the case of the IM-silica network, the linear and branched structures strongly prevail over highly condensed cyclic structures, especially for higher silica contents. This indicates that the presence of the APTMOS component hinders the development of agglomerated SiO_2 structures.

Figure 7 shows the tensile stress–strain curves for the pure PI and both types of hybrid systems, that is, PI/UM-silica and PI/IM-silica hybrid films. The pure PI and U series samples [Fig. 7(a)] exhibit a gradual transition from elastic behavior to plastic behavior without a well-defined yielding point. The tensile strength shows a gradual decrease with increasing silica content in this type of hybrid film, whereas pure PI shows the highest value of 106 MPa. In the case of the PI/IM-silica hybrid series [Fig. 7(b–d)], the tensile strength shows an increasing trend with the increase in the silica content; the opposite behavior can be observed for the PI/UM-silica hybrid series. The presence of the inorganic phase reduces the extent of plastic flow of the PI phase, and consequently, the elongation at break exhibits a decreasing trend with increasing silica content in all four types of hybrid systems. However, the PI/IM-silica series show substantially lower values of the elongation at break than PI/UM-silica hybrids for the same silica concentrations. The tensile modulus values derived from the stress–strain data are reported in Figure 8. The modulus of films for all types of hybrid systems generally increases with an increasing amount of the inorganic phase. However, in comparison with the modulus of pure PI, no enhancement in the modulus of the hybrids is visible until a silica loading of 20 wt % in the case of the PI/UM-silica system and 15 wt % in the case of the PI/IM-silica systems. For the same level of silica content, the PI/IM-silica systems show higher modulus than the PI/UM-silica system. In polymeric composites, the external load transfers from the continuous low-modulus polymer matrix to the discontinuous high-modulus reinforcing filler via a shear stress

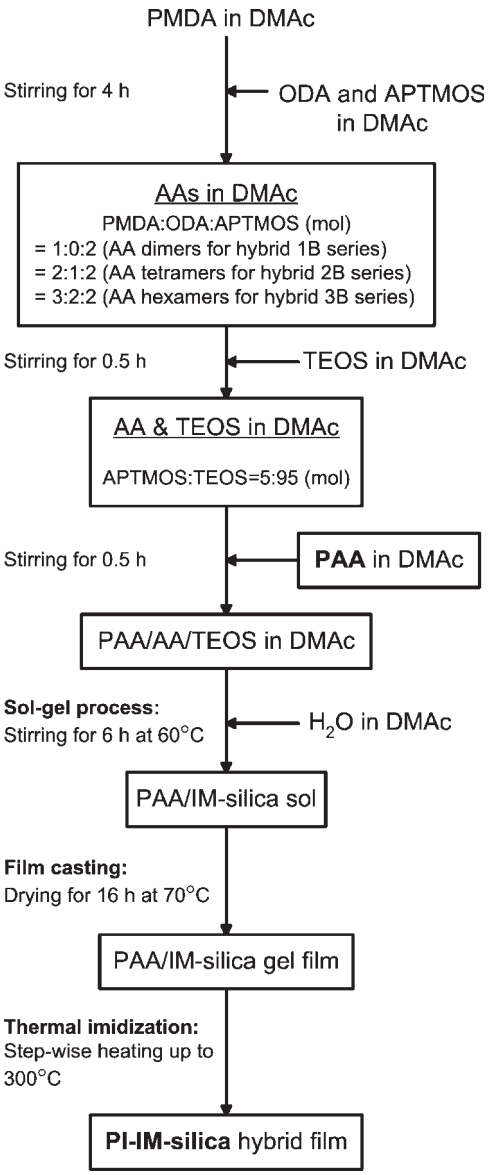

Figure 5 Scheme for the preparation of the PI/IM-silica hybrid (1B, 2B, and 3B series) films.

at the matrix/filler domain interface.[10] For higher shear stress, the filler more efficiently carries the load, and the composite shows higher modulus. The filler may also constrain the mobility of polymer chains in the matrix, thus affecting its modulus. The observed tensile properties of the hybrid films, therefore, indicate an increased extent of adhesion between the phases due to the large surface interaction of the inorganic phase with the matrix.

Figure 9 shows the FESEM micrographs of PI/silica hybrids containing 20 wt % silica. In the case of the PI/UM-silica system [Fig. 9(a)], the dispersed silica particles appear as small beads with an average diameter around 2 μm. This micrograph also reveals that the silica particles are completely detached from the matrix, indicating poor interfacial adhesion. Under the condition of load, such unadhered silica particles act as stress-concentration defects rather than as effective reinforcing components. For the PI/IM-silica systems, the fine interconnected silica domains remain well below 50 nm in size. Well-mixed alkoxysilane-terminated AA oligo- mers in a PAA solution act as nucleation sites for the unsymmetrical growth of silica networks from TEOS during the sol–gel process. A physical network, formed because of the entanglements, between organically active silica networks and high-molecular-weight PAA constrains the phase-separation phenomenon between the PI and inorganic clusters during the imidization stage. The presence of an imide linkage as a spacer group in the silica network prevents the agglomeration of the silica phase.[30] On the basis of these morphological observations [Fig. 9(b–d)], the increased tensile strength in PI/IM-silica

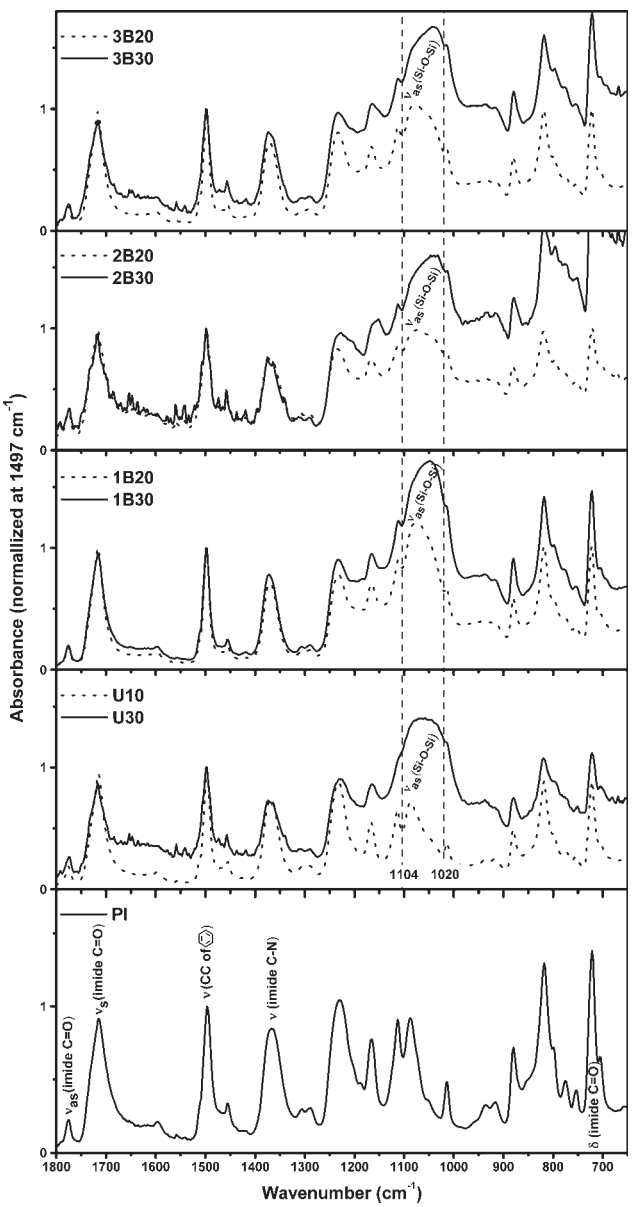

Figure 6 ATR–FTIR spectra of pure PI and PI/silica hybrids.

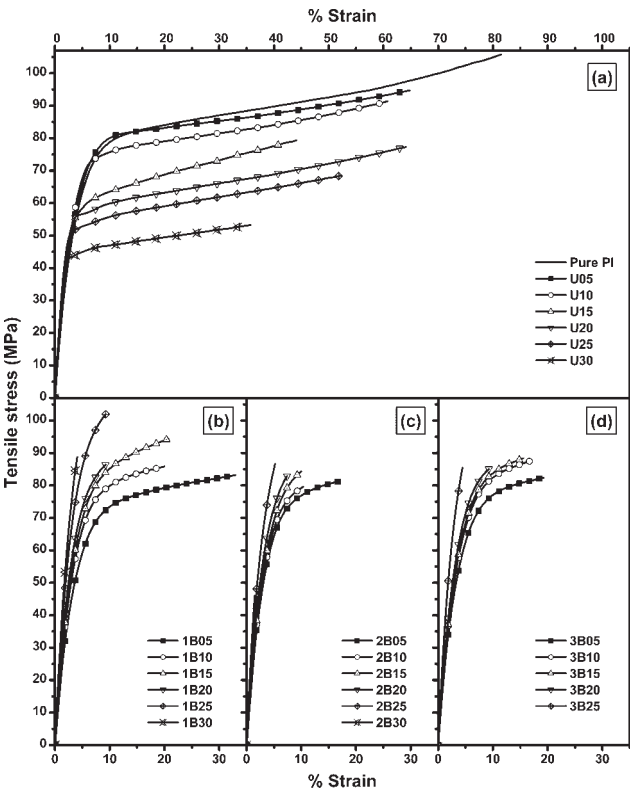

Figure 7 Stress–strain curves of (a) pure PI and U-series hybrids, (b) 1B-series hybrids, (c) 2B-series hybrids, and (d) 3B-series hybrids.

systems can be a result of the reduced size of silica particles and improved interfacial adhesion, which improves the stress-transfer mechanisms between the two components.

To explore the effect of silica-network modification by different-length imide oligomers on the thermal oxidative stability of PI/silica hybrids, we performed a systematic study of all the samples, using a thermogravimetric technique. The assessment is based on the criterion of weight-retention competence of the polymer in the hybrid systems in a thermooxidative environment. From the obtained thermogravimetric data (time, temperature, and mass), the following types of thermal curves were constructed:

1. Principal thermogravimetric analysis (TGA) curve representing the mass percentage (wt %) of a sample as a function of temperature.
2. First derived curve representing the undecomposed fraction $(1 - \alpha)$ as a function of temperature. α is defined as the ratio of the actual weight loss to the total weight loss.
3. Second derived curve representing the time rate of decomposition $(d\alpha/dt)$ as a function of temperature.

The routine, based on the use of linear regression and error analysis originally suggested by Wang et al.,[33] was slightly modified to smoothen the curves. The method provided an effective filter for the noise fluctuations without distorting the TGA data.

Figure 10 shows a set of thermal curves for pure PI and PI/silica hybrids containing 30 wt % silica. Under the experimental conditions, pure PI shows a negligible mass loss (~0.57%) up to 450°C; however, it decomposes completely around 710°C. On the other hand, the PI/silica hybrids containing 30% silica show negligible mass loss (~0.2%) up to 300°C. They lead to a constant mass as a residue, nearly equal to the initial silica loading, at the end of the heating cycle (i.e., 1000°C). The derivative curves [Fig. 10(c)] show that the weight loss in the materials occurs apparently in two stages. However, a small hump in the temperature range of 300–450°C, with a peak value occurring around 400°C, is also visible for PI/silica hybrids only. Such a hump was observed for all the samples containing silica, and its height varied, more or less, with the content of silica and type of silica network. We believe that the appearance of a small hump around 400°C represents the combined effect of additional cyclization and condensation of hydrolyzed silica at elevated temperatures. Therefore, for a more realistic comparison of the stability of materials, we felt it reasonable to eliminate the effect of different degrees of cyclization and silica condensation from the thermal curves. This was done by the consideration of the mass of the specimen at 450°C as the initial mass and by reconstitution of the thermal curves in the temperature range of 450–1000°C (Fig. 11). A comparison of the data on thermooxidative degradation is given in Table II. The following characteristic temperatures were assessed (Fig. 12) for evaluating the thermooxidative response of the samples investigated:

T_{S1} is the temperature corresponding to the onset of intensive decomposition in the first stage.

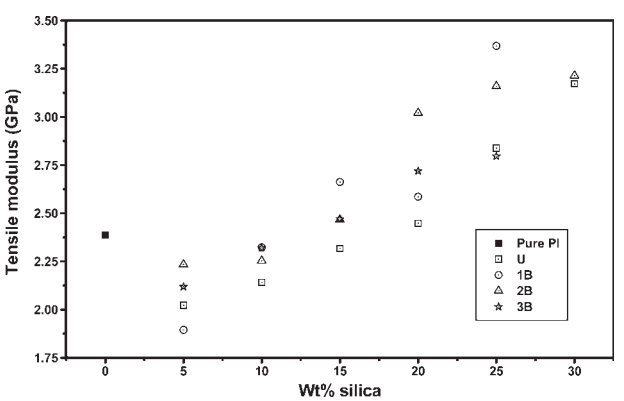

Figure 8 Tensile modulus for pure PI and PI/silica hybrids as a function of the silica content.

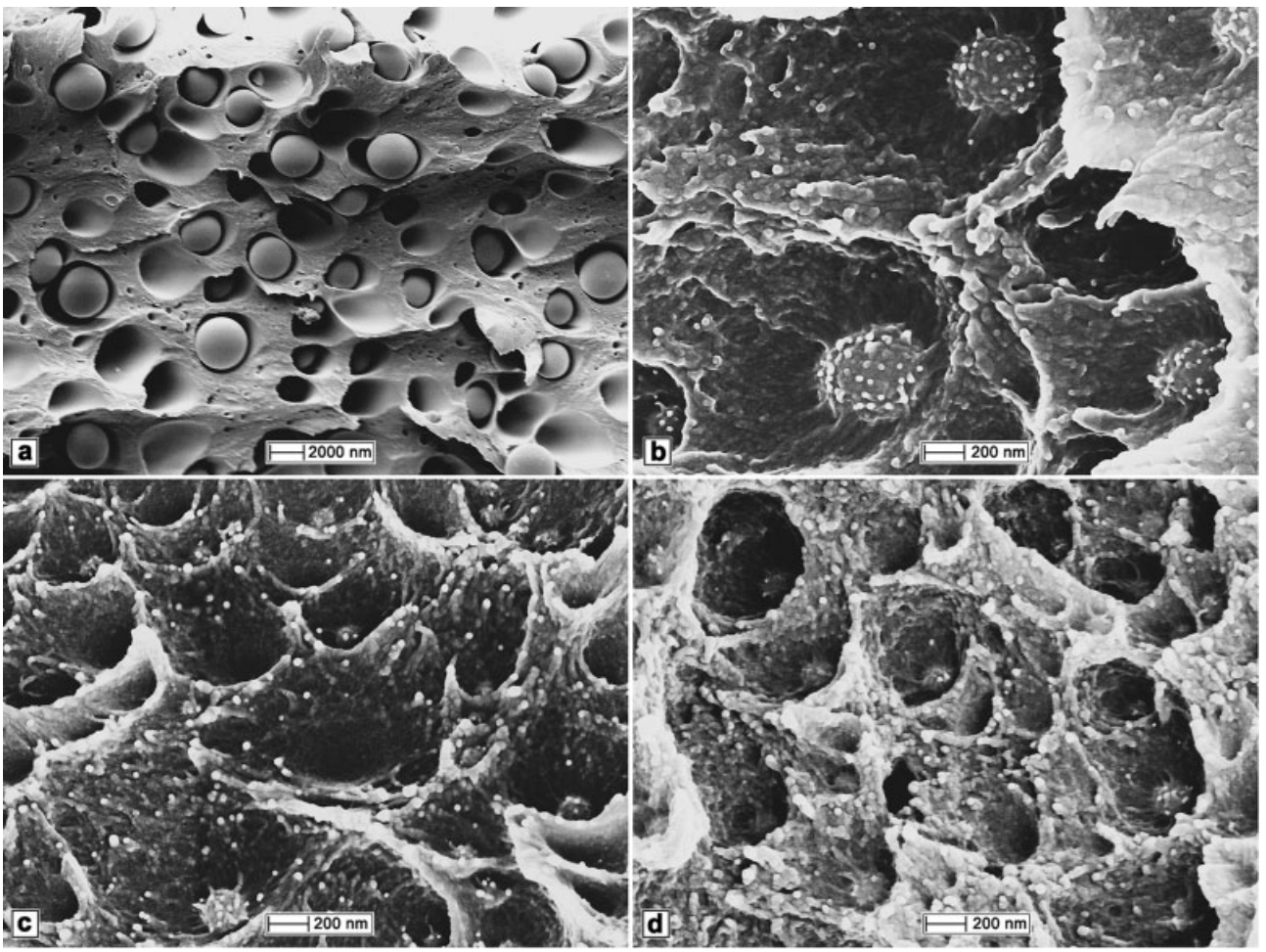

Figure 9 FESEM micrographs for the PI/silica hybrids: (a) U20, (b) 1B20, (c) 2B20, and (d) 3B20.

T_{P1} is the temperature corresponding to the maximum decomposition rate in the first stage.
T_{S2} is the temperature corresponding to the onset of intensive decomposition in the second stage.
T_{P2} is the temperature corresponding to the maximum decomposition rate in the second stage.
T_F is the temperature corresponding to the complete decomposition of the polymer.
$T_{0.5}$ is the temperature corresponding to 50% weight loss of the polymer.

Before a discussion of the thermal oxidative results of this study, it seems useful to mention some important observations put forward by different authors suggesting the decomposition phenomenon of PIs in air and in an inert atmosphere. The decomposition of PIs, over a temperature range from the ambient temperature to ~950°C at a heating rate of 10°C/min, has been reported[34–36] as a single-stage process in a nitrogen atmosphere but a two-stage process in an air atmosphere. The initial reaction step in air or in nitrogen has been found to be very close, and this had led to the conclusion that only the second stage of the decomposition is predominately oxidative in nature. The results of thermoanalytical investigations of PIs reviewed by Sazanov[37] show that under thermooxidative conditions, the PI may entirely transform into volatile products around 650°C, whereas a carbonized residue is formed in an inert atmosphere or *in vacuo* at 900–1000°C. The volatile products consist mainly of CO_2, CO, and H_2O. The C—N bond of the imide ring has been identified as the site of the initial degradation of a PI in air or in an inert atmosphere.[5] The decomposition behavior of PI may change with the incorporation of silica into it. This change can be significant in an oxidative environment as the resulting hybrid morphologies may influence the diffusion rates of oxygen and volatile decomposition products.

The T_{S1} values for PI in hybrids vary in a narrow range (547–566°C) around that of pure PI (557°C). The T_{P1} values show a similar trend and vary in a narrow range (592–617°C) around that of pure PI (607°C). This indicates that the incorporation of silica does not much affect the initiation of polymer degra-

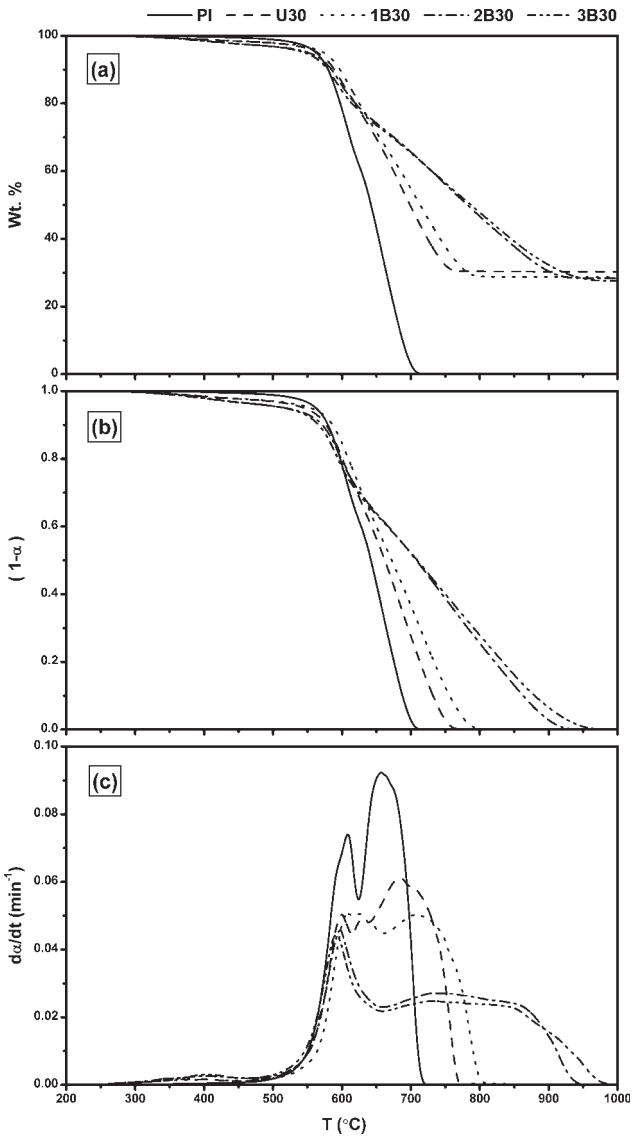

Figure 10 Thermal curves of pure PI and PI/silica hybrids containing 30 wt % silica in the temperature range of 200–1000°C: (a) weight percentage, (b) undecomposed fraction (1 − α), and (c) $d\alpha/dt$.

dation or the first decomposition stage. However, a remarkable change in the characteristic temperatures has been observed during the second stage of decomposition that is predominately oxidative in nature. A comparison of the temperature spans corresponding to two weight-loss stages is shown in Table II. Although the incorporation of silica delays the loss of polymer weight in both stages, this delay is more significant in the second stage. In the U series hybrids, a 10 wt % loading of dispersed silica particles widens the second temperature span up to 220°C in comparison with 88°C for pure PI. For higher silica loadings, the magnitude of the second temperature span gradually decreases, and a 30% silica loading shows a value of 145°C, still much higher than that for pure PI. No change has been observed for a 5 wt % silica loading in this type of hybrid material. On the contrary, for the hybrid series having IM-silica, the completion of the second weight-loss stage is much delayed, even with a 5% silica loading. The hybrids 1B05, 2B05, and 3B05 show second-span values of 174, 182, and 249°C, respectively. For higher silica loadings, the effect is even better, as 1B20, 2B30, and 3B30 show second-span values of 223, 302, and 347°C, respectively.

Thermooxidative stabilization offered by the materials at $\alpha = 0.5$, measured as the difference of the values of $T_{0.5}$ of the polymer (PI) in hybrids and pure PI, is also shown in Table II. A 5 wt % pure silica in hybrid U05 destabilizes the material by 10°C. However, the hybrid U10 shows a maximum stabilization of 44°C that decreases gradually with further silica loading and reaches 22°C for the hybrid U30. On the contrary, having IM-silica, the hybrid 1B05 shows an increase of 35°C in the stabilization temperature, which gradually increases up to 54°C for 1B20 but then decreases to 32°C for hybrid 1B30. The 2B- and 3B-series hybrids show somewhat random behavior. However, an overall increase in stability can be observed with increasing content of IM-silica in these two hybrid series, with the highest values of 72°C for hybrid 2B30 and 74°C for 3B30.

The last column of Table II shows the overall enhancement in the resistance of thermooxidative decomposition of PI upon its reinforcement with UM-silica as well as IM-silica (1B, 2B, and 3B series). In the U series hybrids, the 5 wt % silica loading imparts a small degree of deterioration to the stability of PI. However, all other silica loadings in this series enhance the thermal resistance of the polymer, with a maximum value of 133°C shown by U10 and a minimum of 54°C shown by U30. In the 1B series hybrid system, just 5 wt % silica offers stability of 98°C, which increases gradually with increasing silica content up to 20 wt %, reaches a maximum of 146°C for 1B20, but then decreases to 86°C for hybrid 1B30. The 2B series shows somewhat random behavior; however, a rise of 105°C for 2B05, 159°C for 2B15, and 223°C for 2B30 indicates an increase in the stability trend with an increasing amount of the tetraimide-modified silica component. In the 3B series, the hybrid 3B05 shows a 163°C rise that is the highest among all hybrid systems with the same level of silica loading, that is, 5 wt %. The value decrease a little for 3B10 but again increase gradually for higher silica loadings. A tremendous rise of 262°C can be observed for hybrid 3B30. In general, all compositions in the hybrid series 3B show better weight-retention capabilities of PI at elevated temperatures than the corresponding compositions in the U, 1B, and 2B series.

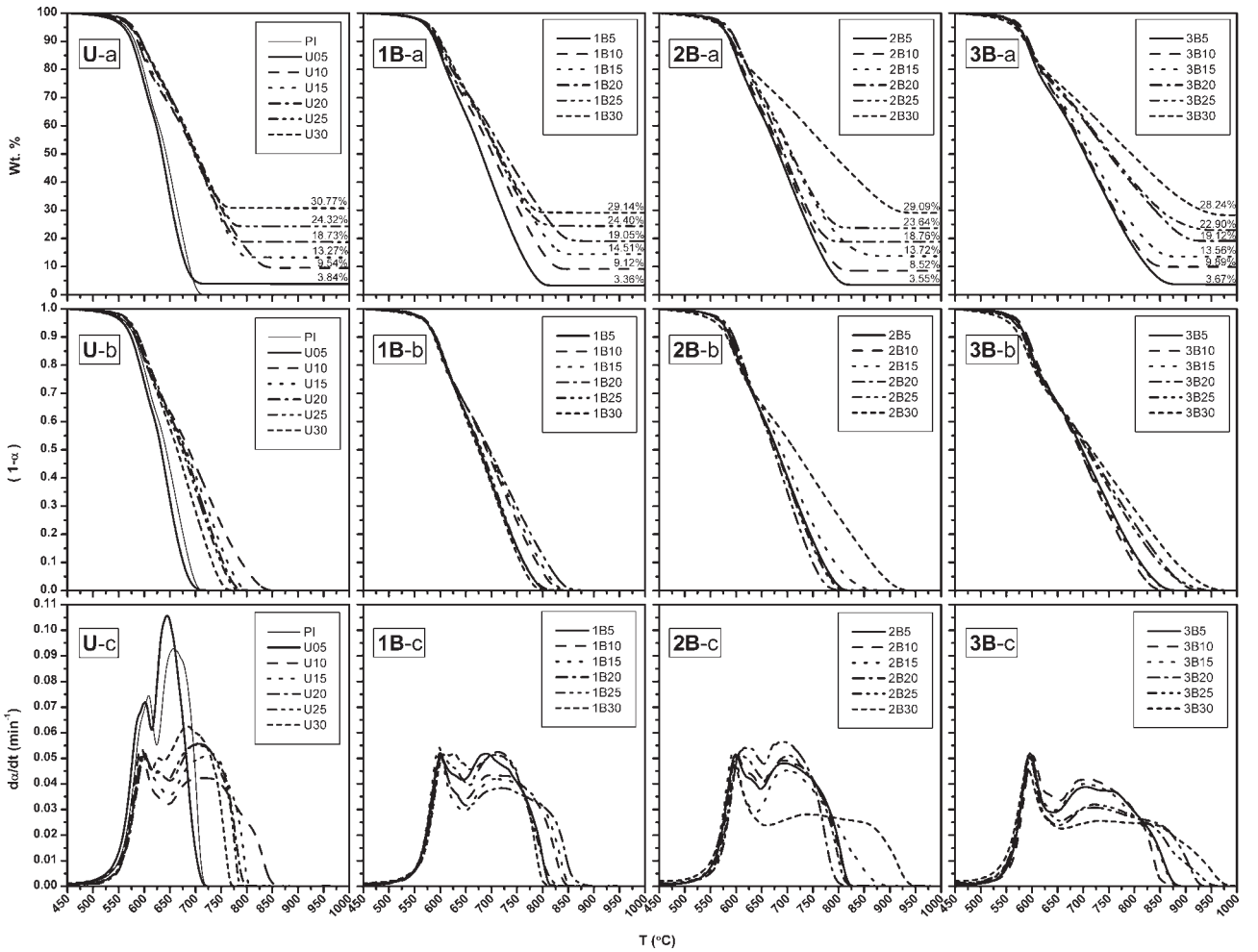

Figure 11 Thermal curves of pure PI and PI/silica hybrids in the temperature range of 450–1000°C: (a) weight percentage, (b) undecomposed fraction ($1 - \alpha$), and (c) $d\alpha/dt$.

The delayed decomposition of the polymer due to the incorporation of nanoscale silica, particularly during the second stage of degradation, indicates that the rate-controlling step may be the diffusion of oxygen in the material. The size of the inorganic phase domains, degree of their distribution and dispersion in the PI matrix, and extent of interfacial interactions are all critical in controlling the transport rates of oxygen into the system and of decomposition products out of the system. The effect of the particle size on the elevated-temperature weight-retention ability of materials is obvious in the U hybrid series, in which increased silica particle size with increasing silica content has lowered the weight retention of PI at elevated temperatures. The hybrid series, having organically modified silica, provide interconnected silica domains separated from one another by chemically bonded imide spacers confined between them. The physically intertwined components of these hybrids may also restrict the segmental motion of PI chains. Such structures act as excellent heat and mass transport barriers, which shift the thermooxidative decomposition profiles toward much higher temperatures. The increase in the imide spacer length not only decreases the size of silica domains but also increases the content of the polymer confined within the silica network. That is why all the compositions in the 3B hybrid series show much better weight-retention abilities at elevated temperatures than the corresponding compositions in the 1B and 2B hybrid series.

CONCLUSIONS

IM-silica network structures having imide oligomers of different chain lengths have been incorporated into a PI matrix to produce PI/silica hybrids. These hybrids provide interconnected silica domains separated from one another by chemically bonded imide spacers. An increase in the spacer length not only decreases the size of silica domains but also increases the content of the polymer confined within the silica network. The hexaimide spacer groups

TABLE II
Characteristic Data Representing the Thermooxidative Response of PI and PI/Silica Hybrids Under Heating from 450 to 1000°C at a Rate of 10°C/min

	Characteristic temperature (°C)						Temperature span (°C)			
Material	T_{S1}	T_{P1}	T_{S2}	T_{P2}	T_F	$T_{0.5}$	First weight-loss stage[a]	Second weight-loss stage[b]	Thermal stabilization at $\alpha = 0.5$ (°C)[c]	Decomposition temperature enhancement (°C)[d]
PI	557	607	625	658	713	643	68	88	—	—
U05	552	598	616	644	704	633	64	88	−10	−9
U10	555	594	626	715	846	687	71	220	44	133
U15	556	597	636	727	802	681	80	166	38	89
U20	556	599	639	702	791	678	83	152	35	78
U25	556	597	633	703	784	674	77	151	31	71
U30	555	598	622	686	767	664	67	145	21	54
1B05	558	600	637	687	811	678	79	174	35	98
1B10	561	600	630	709	841	691	69	211	48	128
1B15	559	597	632	708	848	694	73	216	51	135
1B20	561	600	636	715	859	696	75	223	53	146
1B25	562	603	646	711	816	681	84	170	38	103
1B30	563	607	653	708	799	675	90	146	32	86
2B05	558	598	636	694	818	680	78	182	37	105
2B10	561	600	635	692	816	679	74	181	36	103
2B15	557	594	630	697	872	689	73	242	46	159
2B20	566	617	642	693	792	674	76	150	31	79
2B25	563	608	631	704	812	678	68	181	35	99
2B30	553	598	634	728	936	714	81	302	71	223
3B05	557	596	627	699	876	698	70	249	55	163
3B10	561	600	633	704	851	693	72	218	50	138
3B15	557	595	629	706	873	695	72	244	52	160
3B20	554	595	628	717	925	711	74	297	68	212
3B25	554	595	630	724	951	707	76	321	64	238
3B30	547	592	628	725	975	716	81	347	73	262

[a] $T_{S2} - T_{S1}$.
[b] $T_F - T_{S2}$.
[c] $T_{0.5}$ (hybrid) $- T_{0.5}$ (PI).
[d] T_F (hybrid) $- T_F$ (PI).

thus lead to a hybrid with up to a 262°C increase in the elevated-temperature weight-retention capability of PI. The reinforcement of existing and new PIs by this method offers an opportunity for improving the thermooxidative stability without degrading their mechanical strength.

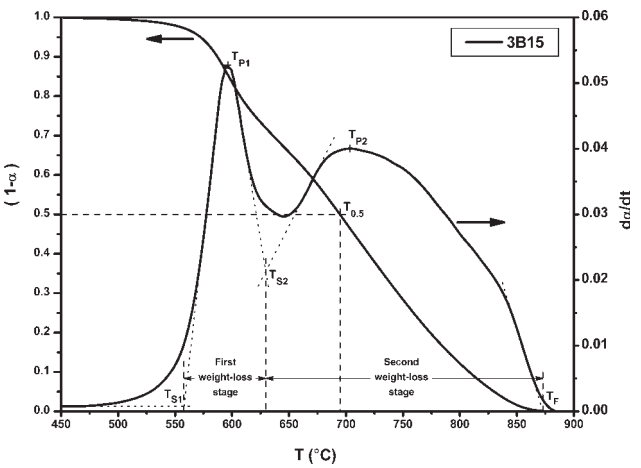

Figure 12 Characteristic temperatures evaluated for the comparison of the thermooxidative response of PI and its hybrid systems.

The authors thank the management of Centralized Resource Laboratory (CRL), University of Peshawar, for providing the facilities to carry out the TGA work.

References

1. Hergenrother, P. M. High Perform Polym 2003, 15, 3.
2. Polyimides and Other High Temperature Polymers; Mittal, K. L., Ed.; VSP: 2003.
3. Sazanov, Y. N. Russ J Appl Chem 2001, 74, 1253.
4. Ghosh, M. K.; Mittal, K. L. Polyimides: Fundamentals and Applications; Marcel Dekker: New York, 1996.
5. Cella, J. A. In Polyimides: Fundamentals and Applications; Ghosh, M. K.; Mittal, K. L., Eds.; Marcel Dekker: New York, 1996; p 343.
6. Kickelbick, G. Prog Polym Sci 2003, 28, 83.
7. Bershtein, V. A.; Egorova, L. M.; Yakushev, P. N.; Pissis, P.; Sysel, P.; Brozova, L. J Polym Sci Part B: Polym Phys 2002, 40, 1056.
8. Alexandre, M.; Dubois, P. Mater Sci Eng Rep 2000, 28, 1.

9. Judeinstein, P.; Sanchez, C. J Mater Chem 1996, 6, 511.
10. Nanocomposite Science and Technology; Ajayan, P. M.; Schadler, L. S.; Braun, P. V., Eds.; Wiley-VCH: Weinheim, 2003.
11. Ahmad, Z.; Mark, J. E. Mater Sci Eng C 1998, 6, 183.
12. Ahmad, Z.; Mark, J. E. Chem Mater 2001, 13, 3320.
13. Wen, J.; Wilkes, G. L. Chem Mater 1996, 8, 1667.
14. Mascia, L. Trends Polym Sci 1995, 3, 61.
15. Wang, S.; Ahmad, Z.; Mark, J. E. Chem Mater 1994, 6, 943.
16. Wang, S.; Ahmad, Z.; Mark, J. E. Macromol Rep A 1994, 31, 411.
17. Schrotter, J. C.; Smaïhi, M.; Guizard, C. J Appl Polym Sci 1996, 61, 2137.
18. Beecroft, L. L.; Johnen, N. A.; Ober, C. K. Polym Adv Technol 1997, 8, 289.
19. Sysel, P.; Pulec, R.; Maryska, M. Polym J 1997, 29, 607.
20. Chen, Y.; Iroh, J. O. Chem Mater 1999, 11, 1218.
21. Wu, K. H.; Chang, T. C.; Wang, Y. T.; Chiu, Y. S. J Polym Sci Part A: Polym Chem 1999, 37, 2275.
22. Cornelius, C. J.; Marand, E. Polymer 2002, 43, 2385.
23. Chang, C.-C.; Wei, K.-H.; Chang, Y.-L.; Chen, W.-C. J Polym Res 2003, 10, 1.
24. Chang, C.-C.; Chen, W.-C. Chem Mater 2002, 14, 4242.
25. Park, H. B.; Kim, J. H.; Kim, J. K.; Lee, Y. M. Macromol Rapid Commun 2002, 23, 544.
26. Yen, C.-T.; Chen, W.-C.; Liaw, D.-J.; Lu, H.-Y. Polymer 2003, 44, 7079.
27. Qiu, F.-X.; Zhou, Y.-M.; Liu, J.-Z. Eur Polym J 2004, 40, 713.
28. Duo, S.; Li, M.; Zhu, M.; Zhou, Y. Surf Coat Technol 2006, 200, 6671.
29. Wahab, M. A.; Ha, C. S. Compos Interfaces 2003, 10, 475.
30. Al-Kandary, S.; Ali, A. A. M.; Ahmad, Z. J Mater Sci 2006, 41, 2907.
31. Al-Kandary, S.; Ali, A. A. M.; Ahmad, Z. J Appl Polym Sci 2005, 98, 2521.
32. Musto, P.; Abbate, M.; Lavorgna, M.; Ragosta, G.; Scarinzi, G. Polymer 2006, 47, 6172.
33. Wang, K.; Wang, S.; Huang, H.; Klein, M. T.; Calkins, W. H. Presented at the 211th National Meeting of the American Chemical Society, New Orleans, LA, 1996.
34. Pramoda, K. P.; Chung, T. S.; Liu, S. L.; Oikawa, H.; Yamaguchi, A. Polym Degrad Stab 2000, 67, 365.
35. Regnier, N.; Guibe, C. Polym Degrad Stab 1997, 55, 165.
36. Torrecillas, R.; Baudry, A.; Dufay, J.; Mortaigne, B. Polym Degrad Stab 1996, 54, 267.
37. Sazanov, Y. N. J Therm Anal 1988, 34, 1117.'